ACS OMEGA

Article

Cite This: ACS Omega 2019, 4, 18593−18599

http://pubs.acs.org/journal/acsodf

Chlorin e6-Conjugated and PEGylated Immune Checkpoint Inhibitor Nanocomposites for Pulmonary Metastatic Colorectal Cancer

Young-IL Jeong,[†] So Young Yoo,*[,†,‡] Jeong Heo,*[,§] and Dae Hwan Kang*[,†]

[†]Research Institute for Convergence of Biomedical Science and Technology, Pusan National University Yangsan Hospital, Yangsan, Gyeongnam 50612, Republic of Korea

[‡]BIO-IT Foundry Technology Institute, Pusan National University, Gumjeong-gu, Busan 46241, Republic of Korea

[§]Department of Internal Medicine and Biomedical Research Institute, Pusan National University Hospital, Seo-gu, Busan 49241, Republic of Korea

Supporting Information

ABSTRACT: Here we demonstrate theranostic immune checkpoint inhibitor nanocomposites (ICI NC) having an improved tumor targeting ability in pulmonary metastatic colon cancer model. Atezolizumab, a PD-L1 antibody, was conjugated with methoxy poly(ethylene glycol) (MePEG) and chlorin e6 (Ce6) via cathepsin-B-sensitive peptide as a linkage (named as ICI nanocomposites, ICI NC). This ICI NC is delivered to tumor sites enriched with tumor-specific enzymes such as cathepsin B, whereas undesired ICI exposure to normal tissue is avoided. When ICI NC were incubated with cathepsin B, Ce6 was released from ICI NC with increased fluorescence intensity in cathepsin B dose-dependent manner, which was by degradation of the peptide and then liberated Ce6 was activated in the aqueous solution. In animal pulmonary metastasis model using CT26 cells, ICI NC showed superior tumor targetability, i.e., fluorescence intensity was significantly strong in the mouse lung having metastatic tumor. On the contrary, cathepsin-B-deficient carriers such as atezolizumab-Ce6 conjugates or atezolizumab-Ce6/MePEG conjugates showed strong fluorescence intensity in the liver as well as lung. Our proposed ICI NC may be used for theranostic cancer therapy with superior tumor specificity of releasing ICI and Ce6 into tumor microenvironment, thereby showing an efficient inhibitory effect on pulmonary metastasis of CT26 cells.

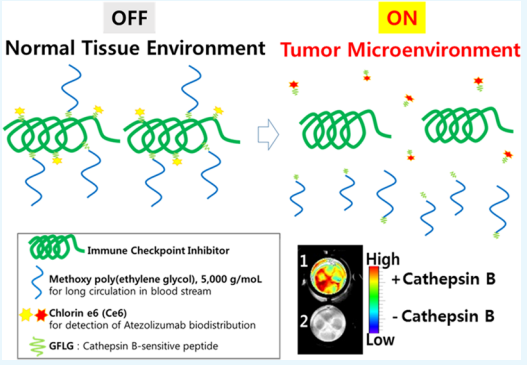

1. INTRODUCTION

Tumors frequently utilize immune checkpoints, a key regulator of the immune system, expressed on themselves and T-cells to disable the immune system killing them.[1,2] Immune system to attack tumor can be restored by blocking these checkpoints.[1,2] Immune checkpoint inhibitors (ICIs) have been extensively investigated in the recent decade since the inhibition of immune checkpoint expression in immune cells or cancer cells is believed to be a more safe and efficient therapeutic regimen for cancer patients than conventional therapy.[3−9] Anticytotoxic T-lymphocyte antigen (CTLA)-4 monoclonal antibody, named as Ipilimumab (Yervoy), was inceptively approved in the US for the first- or second-line treatment option for patients with malignant melanoma.[10] CTLA4, programmed cell death protein 1 (PD-1), and programmed death-ligand 1 (PD-L1) are currently approved for clinical use in treating cancer patients. Upregulation of PD-L1 expression on the tumor cell surface disables T cell activity of 'cancer attack' through binding with PD-1 on an immune cell surface.[11] Therefore, antibodies that bind to either PD-1 of the T cell surface or PD-L1 on the tumor cell surface can elevate antitumor activity of T-cells.[12] Fujimoto et al. reported that nivolumab has reasonable efficacy against patients of metastatic nonsmall-cell lung cancer (NSCLC).[13] Clinical trials using PD-1 and/or PD-L1 inhibitors reported impressive antitumor activity in patients of breast cancer.[14] Furthermore, blocking of PD-L1-induced durable tumor regression and prolonged stabilization of disease in cancer patients, including nonsmall-cell lung cancer, melanoma, and renal cell cancer.[15]

In spite of the successful approach of using ICIs in cancer treatment, various unwanted immune-related adverse events have been reported resulting from the blockade of checkpoints in most of the organs of the human body.[13,16−20] In the clinical use of a PD-1 inhibitor such as nivolumab, pneumonitis is a common immune-related adverse effect, which restricts the clinical use of PD-1 inhibitor for patients of NSCLC.[13] Furthermore, it was reported that immune-related adverse events such as pancreatitis brought severe side effects such as acral vascular necrosis, hypophysitis, and endocrine dysfunction in the clinical use of ICI.[16−20] Researchers are therefore developing novel ICIs to reduce immune-related adverse effects as well as to improve antitumor efficacy for cancer patients.

Received: July 29, 2019
Accepted: October 23, 2019
Published: November 1, 2019

DOI: 10.1021/acsomega.9b02386
ACS Omega 2019, 4, 18593−18599

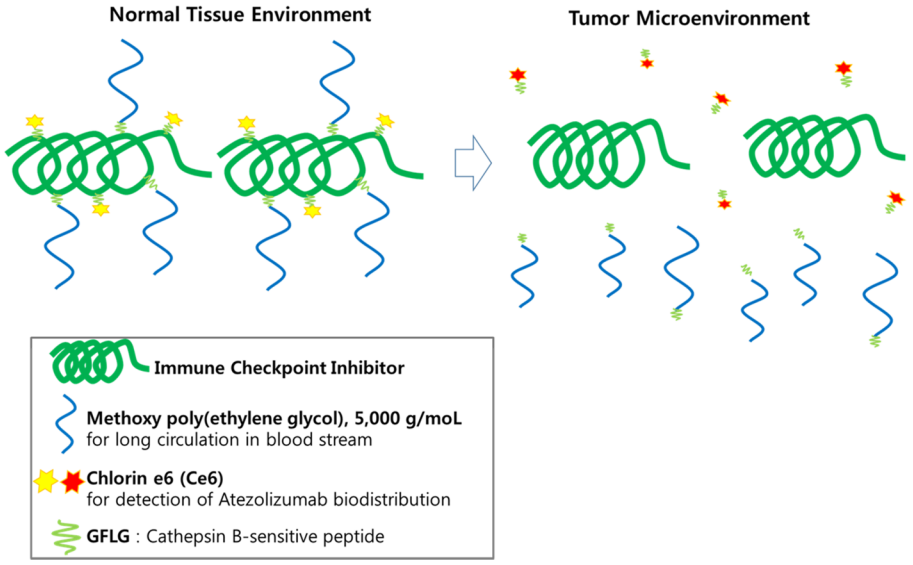

Figure 1. Schematic illustrations of how immune checkpoint inhibitor nanocomposites (ICI NC) can deliver ICI specifically into the tumor microenvironment (TME).

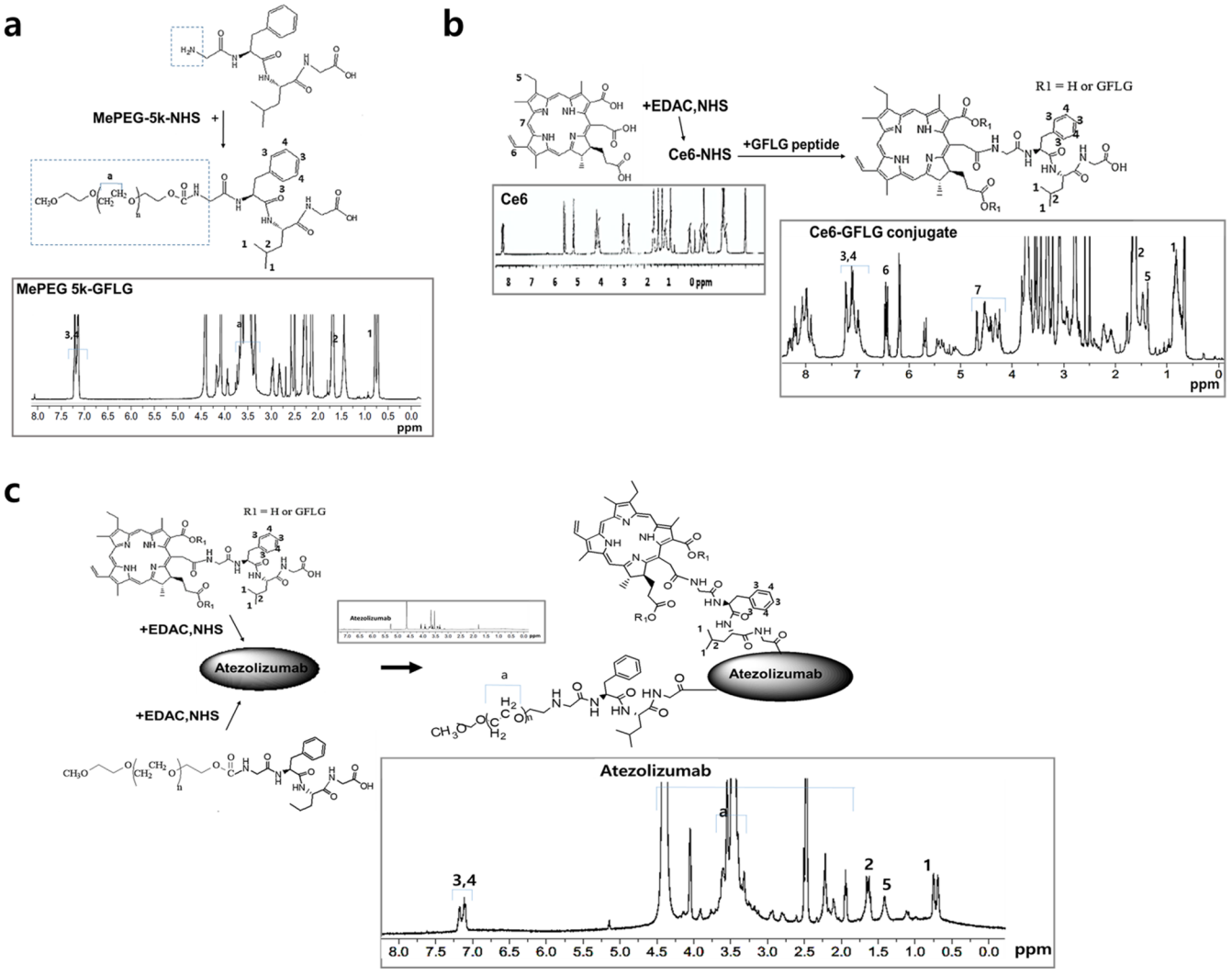

Figure 2. Synthesis scheme and ^{1}H NMR spectra of MePEG-GFLG conjugates (a), Ce6−GFLG conjugates (b), and ICI nanocomposites (c).

Polymer-based drug carriers such as polymer conjugates, nanoparticles, and polymeric micelles have been spotlighted in the targeted drug delivery of bioactive molecules and anticancer drugs.[21−23] They have unique features such as small

DOI: 10.1021/acsomega.9b02386
ACS Omega 2019, 4, 18593−18599

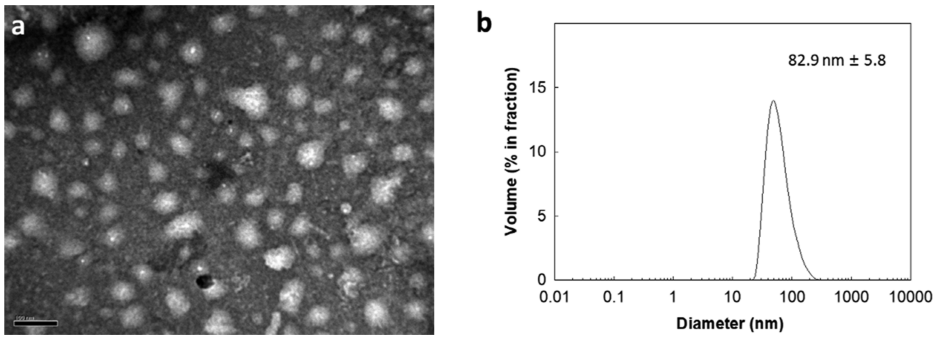

Figure 3. Morphology (a) and particle size distribution (b) of ICI NC. Particle size in the box was average particle sizes ± s.d. from six measurements.

hydrodynamic radius, surface functionality for chemical modification, long-lasting half-lives in the human blood circulation system, and active/passive transport into desirable organs/tissues.[21−25] For example, Lim et al. reported that poly(ethylene glycol)-conjugated anticancer agents via tumor-specific peptide can be specifically delivered to tumor cells by matrix metalloproteases and inhibited viability of cancer cells.[24] Furthermore, transferrin-conjugated polysaccharides deliver anticancer drug to 9L glioma cells in a specific manner.[25] Surface-modified polymer nanoparticles efficiently deliver anticancer agents to liver cancer cells with superior anticancer effects and reduced intrinsic cytotoxicity against normal cells.[26] Song et al. reported that plasmid DNA-loaded lipid nanoparticle delivered PD-L1 trap to cancer cells and oxliplatin/PD-L1 trap combination efficiently inhibited the growth of tumor with reduced immune-related adverse effects.[27] Choo et al. reported that a combination of exosome-mimetic nanovesicles and PD-L1 inhibitors efficiently suppressed tumor growth and potentiated antitumor efficacy of the checkpoint inhibitor therapy.[28] Wang et al. reported that hyaluronidase (HAases) with pH-responsive Dextran for delivering and releasing of HAases in an acidic tumor microenvironment (TME) enhanced the therapeutic effect of photodynamic and PD-L1 checkpoint blockade therapy.[29] Therefore, if we can give tumor targetability and capability of monitoring their work inside the body to ICIs, which can be the best option for successful treatment.

Herein, we demonstrated novel ICI nanocomposites (ICI NC) to be delivered into tumor sites and release ICIs at the sites with fluorescent signal for enhanced immunotherapy of pulmonary metastasis of colon cancer cells (Figure 1). Atezolizumab, a potent PD-L1 inhibitor, was conjugated with methoxy poly(ethylene glycol) (MePEG) and chlorin e6 (Ce6) via cathepsin-B-specific peptide (glycylphenylalanyl-leucylglycine tetrapeptide (Gly-Phe-Leu-Gly, GFLG)) for tumor-specific delivery of atezolizumab. Ce6 produces the fluorescent signal. Since metastatic tumor cells frequently secrete extracellular enzymes such as cathepsin B, cathepsin-B-specific peptide enables vehicles to release and deliver the drug inside to metastatic cancer cells.[30] Anticancer activity of the ICI NC was then investigated using pulmonary metastasis of colon cancer cells.

2. RESULTS AND DISCUSSION

In spite of superior anticancer activity, major drawbacks of ICIs such as CTLA4, PD-1, and PD-L1 are deficiency of tumor specificity, and thus induce immune-related life-threatening adverse effects such as inflammation reaction in all organs.[16,17] In clinical trials, atezolizumab showed a reasonable antitumor activity against metastatic colorectal cancer, metastatic NSCLC, and advanced urothelial carcinomas.[31−33] However, its immune-related adverse effect also was problematic in clinical trials, i.e., grade 3−4 adverse events of atezolizumab-treated group were higher than 30%.[33] From these reasons, tumor specificity of ICI needs to be improved and immune reactions should be reduced in normal organs by the development of novel types of ICI derivatives. Furthermore, in vivo distribution of ICI also needs to be investigated to clarify the immunological reaction of ICI in the human body.

For this purpose, we synthesized ICI NC to assign a tumor-favorable property to ICI. MePEG and Ce6 were conjugated using a cathepsin-B-sensitive peptide linker, as shown in Figure 2. MePEG was introduced in ICI NC due to the stealth properties of PEG.[34] Since PEG is a neutral, flexible, and hydrophilic material, it can form a surface barrier to reduce the adhesion of opsonins and to enhance blood circulation by avoiding an attack of phagocytic cells. Stealth properties of PEG of the nanocarriers give great chances to target TME.[35] Furthermore, Ce6, a potent photosensitizer, enables nanocarriers to diagnose abnormal status of TME.[30] The GFLG tetrapeptide is a widely used linker peptide for drug delivery to cancer, which is sensitive to the lysosomal enzyme, cathepsin B.[36,37] The amide bond between F and L of the peptide is the cleavage sites. Cathepsin B is an emerging therapeutic target protein enriched in TME as well as involved in tumorigenesis and metastasis.[38,39]

Figure 2a shows the synthesis scheme of MePEG−GFLG peptide conjugates. Ethylene protons of PEG were confirmed at 3.6 ppm and specific peaks of GFLG peptide was confirmed at 1.0−7.4 ppm, as shown in Figure 2a, indicating that MePEG−GFLG peptide conjugates were successfully synthesized. Figure 2b shows the synthesis of Ce6−GFLG peptide conjugates. Specific peaks of Ce6 and GFLG peptide were confirmed at 0.8−8.4 ppm, as shown in Figure 2b. The yield of MePEG−GFLG and Ce6−GFLG conjugates was approximately 95 and 96% (w/w), respectively. These were attached to atezolizumab, a PD-L1 inhibitor, as shown in Figure 2c. The molar ratio of MePEG−GFLG conjugates/Ce6−GFLG conjugates/atezolizumab was 4:4:1. As shown in Figure 2c, specific peaks of atezolizumab were confirmed between 1.8 and 5.4 ppm. ^{1}H NMR spectra of ICI NC confirmed that specific peaks of MePEG, GFLG peptide, and Ce6 were assigned at 3.4−3.6, 0.6−0.8 ppm/1.7 ppm/7.1−7.4, and 1.4−1.6 ppm, respectively, indicating that ICI NC were successively synthesized. To estimate chemical structures of PEG−GFLG, Ce6−GFLG conjugates, ICI, and ICI NC, heteronuclear multiple-quantum

DOI: 10.1021/acsomega.9b02386
ACS Omega 2019, 4, 18593−18599

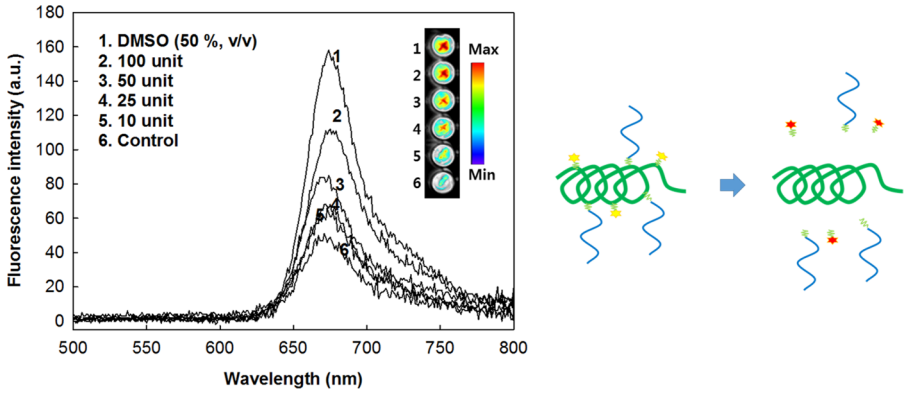

Figure 4. Fluorescence emission spectra and images of ICI nanocomposites in the presence of cathepsin B at different concentrations.

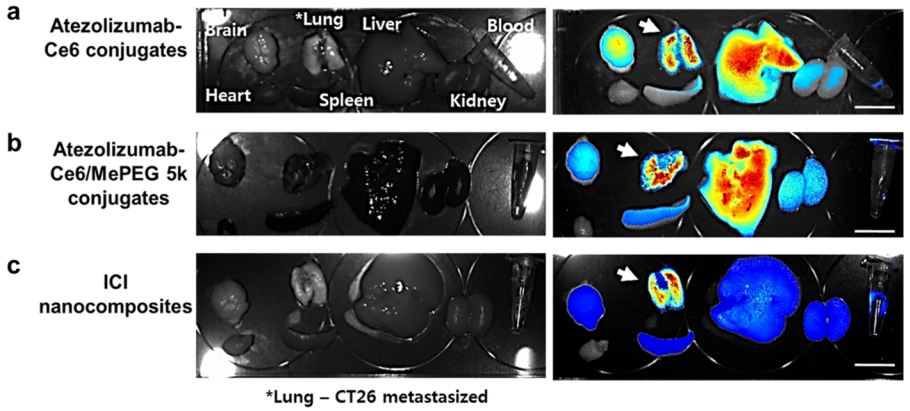

Figure 5. Images of major mouse organs of pulmonary metastasis mouse model using CT26 cells. Dose of each vehicle administrated intravenously (Dose: 20 mg/kg) and, 24 h later, fluorescence images of each organ were observed. (a) Atezolizumab-Ce6 conjugates. (b) Atezolizumab-C36/MePEG 5 k conjugates; absence of GFLG peptide linkage. (c) ICI nanocomposites. (Scale bar = 2 cm).

correlation (HMQC) map using ^{13}C NMR spectra and ^{1}H NMR spectra was performed. As shown in Figure S1, the peak assignments and shifts were confirmed as follows: C1, 20−26 ppm; C2, 23 ppm; and C3 and C4, 130−135 ppm. HMQC of Ce6−GFLG is shown in Figure S2; C1, 21−23 ppm; C2, 25 ppm; C3 and C4, 125−140 ppm; and C6, 120−125 ppm. Figure S3 shows HMQC of ICI (Figure S3a) and ICIC nanocomposites (Figure S3b). Specific peaks of ICI were confirmed at 40−100 ppm in ^{13}C and co-related HMQC map. Furthermore, HMQC map of ICI NC also showed the specific peaks of ICI and PEG. To fabricate nanoparticles, ICI NC were reconstituted in an aqueous solution. ICI NC have spherical shape (Figure 3a) and have a small diameter less than 100 nm (Figure 3b), indicating that ICI NC form self-aggregates in aqueous solution as nanoscale vehicles.

To monitor cathepsin B specificity, ICI NC were incubated with cathepsin B, as shown in Figure 4. Fluorescence intensity of ICI NC was gradually increased according to the dose of cathepsin B, while ICI NC showed strongest fluorescence intensity at dimethylsulfoxide (DMSO) solution (50%, (v/v)). These results indicated that the fluorescent dye, Ce6, was liberated from nanocomposites by the degradation of GFLG peptide and the fluorescence property was activated while Ce6 in the nanocomposites was stayed in the ground state. It was reported that Ce6 in the backbone of nanoparticles stays in the ground state with a weak fluorescence intensity.[30] As Lee et al. showed that the fluorescence intensity of doxorubicin-incorporated nanoparticles increased with incubation with cathepsin B,[40] where the increased fluorescence intensity was due to the cathepsin-B-mediated cleavage of GFLG peptide and then liberation of doxorubicin from nanoparticles, Ce6 was activated and the fluorescence intensity was significantly increased when it was liberated from nanoparticles by degradation of the disulfide bond. Our results confirm the increase of fluorescence intensity with Ce6 liberation from the ICI NC by the treatment of cathepsin B. With Ce6 liberation, atezolizumab is also liberated from the nanocomposites in the TME because cathepsin B is an extracellular enzyme of tumor and closely involved in invasion and metastasis of cancer cells. Linkage of cathepsin-B-sensitive peptide enables nanocarriers to be targeted to metastatic cancer cells specifically. Therefore, our constructed ICI NC may have antitumor activity against metastatic tumor.

To investigate targetability and antitumor activity of ICI NC against tumor metastasis, a pulmonary metastasis model of CT26 colon carcinoma cells was prepared using BALb/C mouse. Figure 5 shows the biodistribution and antitumor activity of ICI NC injected into the mouse model. The delivery capacity of atezolizumab-Ce6 conjugates (Figure 5a), atezolizumab-Ce6/MePEG conjugates (Figure 5b), and ICI nanocomposites (Figure 5c) was compared. All vehicles showed delivery capacity to mouse lung with tumor metastasis. However, GFLG-deficient vehicles such as atezolizumab-Ce6 (Figure 5a) and atezolizumab-Ce6/MePEG conjugates (Figure 5b) showed a strong fluorescence intensity also in the liver. Atezolizumab-Ce6 also showed increased fluorescence intensity in the brain tissues. Importantly, ICI NC (Figure 5c) showed strongest fluorescence intensity in mouse lung with tumor

DOI: 10.1021/acsomega.9b02386
ACS Omega 2019, 4, 18593−18599

metastasis, whereas the fluorescence intensity was relatively decreased at other organs.

These results indicated that our proposed ICI NC have specificity to metastatic tumor cells, while atezolizumab-Ce6 and atezolizumab-Ce6/MePEG conjugates have limited specificity to metastatic tumor. The antitumor activity of ICI NC was then investigated (Figure 6). As expected, improved

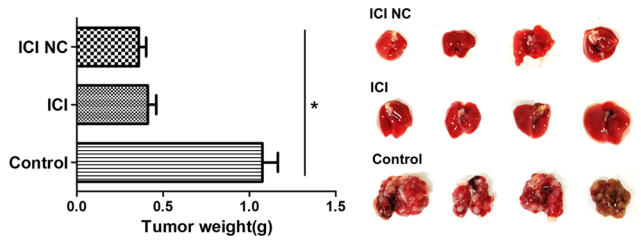

Figure 6. Tumor weight measurement of mouse model of pulmonary metastatis of CT26 cells. The dose of each vehicle administrated was 20 mg/kg. * $p < 0.0001$, one-way ANOVA.

tumor targetability of ICI NC enhanced the therapeutic activity of ICI, and ICI NC efficiently inhibited metastasis of CT26 cells, i.e., the lung weight of ICI NC treated mice group was approximately 30% of the control group (Control > ICI > ICI NC, *$p < 0.0001$, one-way analysis of variance (ANOVA)).

Taken all together, ICI NC have superior targetability to metastasis tumor and efficiently inhibited metastasis of tumor cells. Released Ce6 with ICIs at the sites showed strong fluorescent signal to be monitored. Therefore, our experimental model of ICI NC has superior antitumor activity and targetability against metastatic tumor, proposing a novel ICI NC for the next onco-immuno-therpeutics to modulate TME and kill metastatic cancer.

3. CONCLUSIONS

We demonstrated ICI NC having improved tumor targetability. MePEG and Ce6 were conjugated with atezolizumab using cathepsin-B-sensitive peptide as a linkage (ICI nanocomposites). They have small sizes as nanocarriers and showed cathepsin-B-sensitive liberation of Ce6, indicating that ICI NC can be delivered in a cathepsin-B-sensitive manner in the TME. In the animal tumor metastasis model using CT26 cells, ICI NC showed superior targetability with a fluorescent signal monitor against pulmonary metastasis of CT26 colorectal cells and efficiently inhibited metastasis of tumor, without sacrificing ICI antibody's own activity as well as without worrying about unexpected side effects at normal tissues.

4. EXPERIMENTAL SECTION

4.1. Materials. Atezolizumab was purchased from Selleckchem Co. Ltd. (Huston, TX). Methoxy poly(ethylene glycol)-succinimidylglutarate (MePEG−NHS, molecular weight (M.W.): 5000 g/mol) was purchased from SunBio Co. Ltd. (Seoul, S. Korea). GFLG tetrapeptide was purchased from Peptron Co (Daejeon, S. Korea). The dialysis membranes with molecular-weight cutoffs (MWCO) of 1000, 2000, and 8000 g/mol were purchased from Spectra/ProTM Membranes (New Brunswick, NJ). Chlorin e6 (Ce6) was purchased from Frontier Scientific Inc. (Logan, UT). Phosphotungstic acid, *N*-(3-dimethylaminopropyl)-*N*′-ethylcarbodiimide hydrochloride (EDAC), *N*-hydroxysuccinimide (NHS), triethylamine, cathepsin B (from bovine spleen), and dimethylsulfoxide (DMSO) were purchased from Sigma Chem. Co. (St. Louis, MO). Organic solvents such as methanol were used as high-performance liquid chromatography grade or extra-pure grade.

4.2. Synthesis of PEGylated ICI−Ce6 Conjugates. MePEG−GFLG peptide conjugates: 500 mg of MePEG−NHS dissolved in 9 mL of DMSO was mixed with 1.2 equiv mole of GFLG peptide (47 mg) in 1 mL of H_2O and then magnetically stirred for 24 h. After that, reactants were introduced into the dialysis membrane (MWCO: 2000 g/mol). These were dialyzed against deionized water to remove organic solvent and unreacted chemicals for 2 days. Water was changed every 2−3 h intervals. The resulting solution was lyophilized for 2 days. The yield was measured by mass measurement. The yield was approximately 95% (w/w). Yield = [weight of final product/(weight of MePEG−NHS + GFLG peptide)] × 100.

4.2.1. Ce6−GFLG Peptide Conjugates. Ce6 (60 mg) dissolved in 9 mL of DMSO was mixed with 2 equiv mole of GFLG peptide in 2 mL of H_2O. These mixtures were magnetically stirred for 36 h and then introduced into the dialysis membrane (MWCO: 1000 g/mol). These were dialyzed against deionized water to remove organic solvent and unreacted chemicals for 2 days. Water was changed every 2−3 h intervals. The resulting solution was lyophilized for 2 days. The yield was higher than 96% (w/w). Yield = [weight of final product/(weight of Ce6 + GFLG peptide)] × 100.

4.2.2. Atezolizumab-Ce6 Conjugates. To make NHS-activated Ce6, Ce6 (2.4 mg) in 2 mL of DMSO was activated with 1 equiv mole of EDAC and NHS. These were magnetically stirred for 24 h. Following this, 145 mg of atezolizumab in 10 mL of phosphate-buffered saline (PBS, pH 7.4, 0.01 M) was mixed with 2 mL of NHS-activated Ce6 and then introduced into the dialysis membrane (MWCO: 8000 g/mol). These were dialyzed against deionized water to remove organic solvent and unreacted chemicals for 2 days at 4 °C. Water was changed every 2−3 h intervals. The resulting solution was lyophilized for 2 days. Ce6 contents were approximately 1.4% (w/w).

4.2.3. Atezolizumab-Ce6/MePEG Conjugates. To make NHS-activated Ce6, Ce6 (2.4 mg) in 2 mL of DMSO was activated with 1 equiv mole of EDAC and NHS. These were magnetically stirred for 24 h. Following this, 145 mg of atezolizumab in 10 mL of phosphate-buffered saline (PBS, pH 7.4, 0.01 M) was mixed with 2 mL of NHS-activated Ce6 and 20 mg MePEG−NHS. These mixtures were magnetically stirred for 12 h and then introduced into the dialysis membrane (MWCO: 8000 g/mol). These were dialyzed against deionized water to remove organic solvent and unreacted chemicals for 2 days at 4 °C. Water was changed every 2−3 h intervals. The resulting solution was lyophilized for 2 days. Ce6 contents were approximately 1.23% (w/w).

4.2.4. ICI Nanocomposites. MePEG−GFLG peptide (216 mg) in 10 mL of DMSO was mixed with 3.8 mg of EDAC and 2.3 mg of NHS to make NHS-activated MePEG−GFLG peptide. These were magnetically stirred for 24 h. Ce6−GFLG peptide conjugates (53 mg) in 20 mL of DMSO were also activated with 7.7 mg of EDAC and 4.6 mg of NHS to make NHS-activated Ce6−GFLG peptide conjugates. These were magnetically stirred for 24 h. Following this, 145 mg of atezolizumab in 10 mL of phosphate-buffered saline (PBS, pH 7.4, 0.01 M) was mixed with 1 mL of NHS-activated MePEG−GFLG peptide and 2 mL of NHS-activated Ce6−GFLG peptide conjugates. These mixtures were magnetically stirred for 12 h and then introduced into the dialysis membrane

DOI: 10.1021/acsomega.9b02386
ACS Omega 2019, 4, 18593−18599

(MWCO: 8000 g/mol). These were dialyzed against deionized water to remove organic solvent and unreacted chemicals for 2 days at 4 °C. Water was changed every 2−3 h intervals. The resulting solution was lyophilized for 2 days. Ce6 contents were approximately 1.21% (w/w). Ce6 contents were measured as follows: 10 mg of conjugates were reconstituted in 2 mL of deionized water and mixed with 8 mL of DMSO. This solution was appropriately diluted with DMSO. Ce6 concentration was evaluated with an Infinite M200pro microplate reader (Tecan) (excitation wavelength: 407, emission wavelength: 664 nm). Ce6 itself dissolved in DMSO was used for the standard test. Ce6 content (wt %) = (Ce6 weight/total weight of conjugates) × 100.

4.2.5. ^{13}C NMR Spectra. The chemical structure of ICI nanocomposites was confirmed with ^{13}C NMR spectra (500 mHz superconducting Fourier transform (FT)-NMR spectrometer, Varian Unity Inova 500 MHz NB High Resolution FT NMR; Varian Inc, Santa Clara, CA).

4.3. Characterization of PEGylated ICI Nanocomposites. Synthesis of ICI nanocomposites and each chemical was monitored with ^{1}H NMR spectra (500 mHz superconducting Fourier transform (FT)-NMR spectrometer, Varian Unity Inova 500 MHz NB High Resolution FT NMR; Varian Inc, Santa Clara, CA). Synthesized ICI nanocomposites were reconstituted in an aqueous solution such as deionized water or PBS (pH 7.4, 0.01 M) by brief sonication. Particle sizes of ICI nanocomposites (0.1%, w/w) were measured with Zetasizer Nano-ZS (Malvern, Worcestershire, U.K.). Morphology of nanocomposites was observed with a transmission electron microscope (TEM) (H-7600, Hitachi Instruments Ltd., Tokyo, Japan). The nanocomposite solution was placed on the carbon-film-coated grid for TEM and then dried in room temperature for 3 h. Nanocomposites were stained negatively with phosphotungstic acid (0.1%, w/w in deionized water). The observation was carried out at 80 kV.

Fluorescence emission scan between 500 and 800 nm (excitation wavelength: 400 nm) was measured with a multifunctional microplate reader (Infinite M200pro microplate reader, Tecan, Mannedorf, Switzerland). The same solution was fluorescently observed with Maestro 2 small animal imaging instrument (Cambridge Research and Instrumentation Inc., Hopkinton, MA). To analyze Ce6 liberation, 5 mg of ICI nanocomposites was reconstituted in 2.5 mL of phosphate-buffered saline (PBS, pH 7.4, 0.01 M) and then mixed with various concentrations of cathepsin B. This solution was incubated for 3 h at 37 °C and then used for fluorescence scan.

4.4. Cell Culture. CT26 mouse colorectal carcinoma cells were obtained from the Korean Cell Line Bank Co. (Seoul < Korea). Cells were maintained with Roswell Park Memorial Institute (RPMI)-1640 medium supplemented with 10% (v/v) fetal bovine serum and 1% (v/v) antibiotics in a 5% CO_2 incubator (37 °C).

4.5. In Vivo Pulmonary Metastasis of Colon Cancer. Pulmonary metastasis of CT26 cells were prepared using BALb/C mice (male, 20 g, 4 weeks old). CT26 cells (1 × 105 cells/0.1 mL) was intravenously (i.v.) administered via the tail vein. Four mice were used for each group. Three days later, ICI nanocomposites reconstituted in PBS were sterilized with a 1.2 μm syringe filter and then i.v. injected into the mice (Dose: 20 mg/kg). For control treatment, PBS was injected. The injection volume was 0.2 mL. After 2 weeks, the mice were sacrificed to separate each organ and to measure the weight of the lungs. The fluorescence imaging of mice pulmonary metastasis of CT26 cells was performed as follows. ICI nanocomposites (injection volume: 0.2 mL, dose: 20 mg/kg) were administered into the tail vein of BALb/C mice (0.2 mL). For comparison, atezolizumab-Ce6 conjugates and atezolizumab-Ce6/MePEG conjugates were also i.v. administered. Injection volumes and dose were 0.2 mL and 20 mg/kg. The injection dose of each conjugate was based on ICI. Twenty-four hours later, the mice were sacrificed to observe each organ with a Maestro 2TM in vivo imaging system (Cambridge Research and Instruments, Inc., Woburn, MA01801) at 780 nm. Animal experiments in this study were carried out based on the guidelines of the Pusan National University Institutional Animal Care and Use Committee (PNUIACUC). Experimental protocol of animal study was strictly reviewed by PNUIACUC in terms of ethical procedures and scientific care and approved (approval number: PNU-2017-1610).

■ ASSOCIATED CONTENT

Supporting Information

The Supporting Information is available free of charge on the ACS Publications website at DOI: 10.1021/acsomega.9b02386.

$^{13}C-^{1}H$ single bond correlation (HMQC) of PEG-GFLG conjugates; Ce6-GFLG conjugates; ICI (Atezolizumab) and ICI nanocomposites (PDF)

■ AUTHOR INFORMATION

Corresponding Authors

*E-mail: yoosy@pusan.ac.kr, yoosy2@gmail.com (S.Y.Y.).
*E-mail: sodium@korea.com (J.H.).
*E-mail: sulsulpul@naver.com (D.H.K.).

ORCID

So Young Yoo: 0000-0001-8875-9289

Author Contributions

Y.-L.J. and S.Y.Y. contributed equally to this work. The manuscript was written through contributions of all authors. All authors have given approval to the final version of the manuscript.

Notes

The authors declare no competing financial interest.

■ ACKNOWLEDGMENTS

This study was supported by the Biomedical Research Institute Grant and Busan Cancer Center Grant (2018B041), Pusan National University Hospital.

■ REFERENCES

(1) Ishida, Y.; Agata, Y.; Shibahara, K.; Honjo, T. Induced expression of PD-1, a novel member of the immunoglobulin gene superfamily, upon programmed cell death. *EMBO J.* **1992**, *11*, 3887−3895.

(2) Nishimura, H.; Minato, N.; Nakano, T.; Honjo, T. Immunological studies on PD-1 deficient mice: implication of PD-1 as a negative regulator for B cell responses. *Int. Immunol.* **1998**, *10*, 1563−1572.

(3) Iwai, Y.; Hamanishi, J.; Chamoto, K.; Honjo, T. Cancer immunotherapies targeting the PD-1 signaling pathway. *J. Biomed. Sci.* **2017**, *24*, No. 26.

(4) Chowdhury, P. S.; Chamoto, K.; Honjo, T. Combination therapy strategies for improving PD-1 blockade efficacy: a new era in cancer immunotherapy. *J. Intern. Med.* **2018**, *283*, 110−120.

(5) Pardoll, D. M. The blockade of immune checkpoints in cancer immunotherapy. *Nat. Rev. Cancer* **2012**, *12*, 252−264.

DOI: 10.1021/acsomega.9b02386
ACS Omega 2019, 4, 18593−18599

(6) Zhu, X.; Lang, J. Programmed death-1 pathway blockade produces a synergistic antitumor effect: combined application in ovarian cancer. *J. Gynecol. Oncol.* **2017**, *28*, No. e64.
(7) Szostak, B.; Machaj, F.; Rosik, J.; Pawlik, A. CTLA4 antagonists in phase I and phase II clinical trials, current status and future perspectives for cancer therapy. *Expert Opin. Invest. Drugs* **2019**, *28*, 149−159.
(8) Alsharedi, M.; Katz, H. Check point inhibitors a new era in renal cell carcinoma treatment. *Med. Oncol.* **2018**, *35*, No. 85.
(9) Darvin, P.; Toor, S. M.; Sasidharan Nair, V.; Elkord, E. Immune checkpoint inhibitors: recent progress and potential biomarkers. *Exp. Mol. Med.* **2018**, *50*, No. 165.
(10) Cameron, F.; Whiteside, G.; Perry, C. Ipilimumab: first global approval. *Drugs* **2011**, *71*, 1093−1104.
(11) Karwacz, K.; Bricogne, C.; MacDonald, D.; Arce, F.; Bennett, C. L.; Collins, M.; Escors, D. PD-L1 co-stimulation contributes to ligand-induced T cell receptor down-modulation on CD8+ T cells. *EMBO Mol. Med.* **2011**, *3*, 581−592.
(12) Syn, N. L.; Teng, M. W. L.; Mok, T. S. K.; Soo, R. A. De-novo and acquired resistance to immune checkpoint targeting. *Lancet Oncol.* **2017**, *18*, e731−e741.
(13) Fujimoto, D.; Morimoto, T.; Ito, J.; Sato, Y.; Ito, M.; Teraoka, S.; Otsuka, K.; Nagata, K.; Nakagawa, A.; Tomii, K. A pilot trial of nivolumab treatment for advanced non-small cell lung cancer patients with mild idiopathic interstitial pneumonia. *Lung Cancer* **2017**, *111*, 1−5.
(14) Bertucci, F.; Goncalves, A. Immunotherapy in Breast Cancer: the Emerging Role of PD-1 and PD-L1. *Curr. Oncol. Rep.* **2017**, *19*, No. 64.
(15) Brahmer, J. R.; Tykodi, S. S.; Chow, L. Q.; Hwu, W. J.; Topalian, S. L.; Hwu, P.; Drake, C. G.; Camacho, L. H.; Kauh, J.; Odunsi, K.; Pitot, H. C.; Hamid, O.; Bhatia, S.; Martins, R.; Eaton, K.; Chen, S.; Salay, T. M.; Alaparthy, S.; Grosso, J. F.; Korman, A. J.; Parker, S. M.; Agrawal, S.; Goldberg, S. M.; Pardoll, D. M.; Gupta, A.; Wigginton, J. M. Safety and activity of anti-PD-L1 antibody in patients with advanced cancer. *N. Engl. J. Med.* **2012**, *366*, 2455−2465.
(16) Postow, M. A.; Sidlow, R.; Hellmann, M. D. Immune-Related Adverse Events Associated with Immune Checkpoint Blockade. *N. Engl. J. Med.* **2018**, *378*, 158−168.
(17) Friedman, C. F.; Snyder, A. Atypical autoimmune adverse effects with checkpoint blockade therapies. *Ann. Oncol.* **2017**, *28*, 206−207.
(18) George, J.; Bajaj, D.; Sankaramangalam, K.; Yoo, J. W.; Joshi, N. S.; Gettinger, S.; Price, C.; Farrell, J. J. Incidence of pancreatitis with the use of immune checkpoint inhibitors (ICI) in advanced cancers: A systematic review and meta-analysis. *Pancreatology* **2019**, *19*, 587−594.
(19) Khaddour, K.; Singh, V.; Shayuk, M. Acral vascular necrosis associated with immune-check point inhibitors: case report with literature review. *BMC Cancer* **2019**, *19*, No. 449.
(20) Joshi, M. N.; Whitelaw, B. C.; Palomar, M. T.; Wu, Y.; Carroll, P. V. Immune checkpoint inhibitor-related hypophysitis and endocrine dysfunction: clinical review. *Clin. Endocrinol.* **2016**, *85*, 331−339.
(21) Wadhwa, S.; Mumper, R. J. Polymer-Drug Conjugates for Anticancer Drug Delivery. *Crit. Rev. Ther. Drug Carrier Syst.* **2015**, *32*, 215−245.
(22) Nicolas, J.; Couvreur, P. Polymer nanoparticles for the delivery of anticancer drug. *Med. Sci.* **2017**, *33*, 11−17.
(23) Matsumura, Y. Preclinical and clinical studies of anticancer drug-incorporated polymeric micelles. *J. Drug Targeting* **2007**, *15*, 507−517.
(24) Lim, S. H.; Jeong, Y. I.; Moon, K. S.; Ryu, H. H.; Jin, Y. H.; Jin, S. G.; Jung, T. Y.; Kim, I. Y.; Kang, S. S.; Jung, S. Anticancer activity of PEGylated matrix metalloproteinase cleavable peptide-conjugated adriamycin against malignant glioma cells. *Int. J. Pharm.* **2010**, *387*, 209−214.
(25) Jeong, Y. I.; Kim, Y. W.; Jung, S.; Pei, J.; Wen, M.; Li, S. Y.; Ryu, H. H.; Lim, J. C.; Jang, W. Y.; Kim, I. Y.; Moon, K. S.; Jung, T. Y. Delivery of Transferrin-Conjugated Polysaccharide Nanoparticles in 9L Gliosacoma Cells. *J. Nanosci. Nanotechnol.* **2015**, *15*, 125−129.
(26) Song, X.; Wang, J.; Xu, Y.; Shao, H.; Gu, J. Surface-modified PLGA nanoparticles with PEG/LA-chitosan for targeted delivery of arsenic trioxide for liver cancer treatment: Inhibition effects enhanced and side effects reduced. *Colloids Surf., B* **2019**, *180*, 110−117.
(27) Song, W.; Shen, L.; Wang, Y.; Liu, Q.; Goodwin, T. J.; Li, J.; Dorosheva, O.; Liu, T.; Liu, R.; Huang, L. Synergistic and low adverse effect cancer immunotherapy by immunogenic chemotherapy and locally expressed PD-L1 trap. *Nat. Commun.* **2018**, *9*, No. 2237.
(28) Choo, Y. W.; Kang, M.; Kim, H. Y.; Han, J.; Kang, S.; Lee, J. R.; Jeong, G. J.; Kwon, S. P.; Song, S. Y.; Go, S.; Jung, M.; Hong, J.; Kim, B. S. M1 Macrophage-Derived Nanovesicles Potentiate the Anticancer Efficacy of Immune Checkpoint Inhibitors. *ACS Nano* **2018**, *12*, 8977−8993.
(29) Wang, H.; Han, X.; Dong, Z.; Xu, J.; Wang, J.; Liu, Z. Hyaluronidase with pH-responsive Dextran Modification as an Adjuvant Nanomedicine for Enhanced Photodynamic-Immunotherapy of Cancer. *Adv. Funct. Mater.* **2019**, *29*, No. 1902440.
(30) Lee, S.-J.; Jeong, Y.-I. L. Hybrid nanoparticles based on chlorin e6-conjugated hyaluronic acid/poly(l-histidine) copolymer for theranostic application to tumors. *J. Mater. Chem. B* **2018**, *6*, 2851−2859.
(31) Tapia Rico, G.; Price, T. J. Atezolizumab for the treatment of colorectal cancer: the latest evidence and clinical potential. *Expert Opin. Biol. Ther.* **2018**, *18*, 449−457.
(32) Horn, L.; Gettinger, S. N.; Gordon, M. S.; Herbst, R. S.; Gandhi, L.; Felip, E.; Sequist, L. V.; Spigel, D. R.; Antonia, S. J.; Balmanoukian, A.; Cassier, P. A.; Liu, B.; Kowanetz, M.; O'Hear, C.; Fasso, M.; Grossman, W.; Sandler, A.; Soria, J. C. Safety and clinical activity of atezolizumab monotherapy in metastatic non-small-cell lung cancer: final results from a phase I study. *Eur. J. Cancer* **2018**, *101*, 201−209.
(33) Eng, C.; Kim, T. W.; Bendell, J.; Argiles, G.; Tebbutt, N. C.; Di Bartolomeo, M.; Falcone, A.; Fakih, M.; Kozloff, M.; Segal, N. H.; Sobrero, A.; Yan, Y.; Chang, I.; Uyei, A.; Roberts, L.; Ciardiello, F.; et al. Atezolizumab with or without cobimetinib versus regorafenib in previously treated metastatic colorectal cancer (IMblaze370): a multicentre, open-label, phase 3, randomised, controlled trial. *Lancet Oncol.* **2019**, *20*, 849−861.
(34) Salmaso, S.; Caliceti, P. Stealth Properties to Improve Therapeutic Efficacy of Drug Nanocarriers. *J. Drug Delivery* **2013**, *2013*, No. 374252.
(35) Li, S. D.; Huang, L. Stealth nanoparticles: high density but sheddable PEG is a key for tumor targeting. *J. Controlled Release* **2010**, *145*, 178−181.
(36) Chu, T. W.; Yang, J.; Kopecek, J. Anti-CD20 multivalent HPMA copolymer-Fab' conjugates for the direct induction of apoptosis. *Biomaterials* **2012**, *33*, 7174−7181.
(37) Yang, N.; Ye, Z.; Li, F.; Mahato, R. I. HPMA polymer-based site-specific delivery of oligonucleotides to hepatic stellate cells. *Bioconjugate Chem.* **2009**, *20*, 213−221.
(38) Bian, B.; Mongrain, S.; Cagnol, S.; Langlois, M. J.; Boulanger, J.; Bernatchez, G.; Carrier, J. C.; Boudreau, F.; Rivard, N. Cathepsin B promotes colorectal tumorigenesis, cell invasion, and metastasis. *Mol. Carcinog.* **2016**, *55*, 671−687.
(39) Reinheckel, T.; Peters, C.; Krüger, A.; Turk, B.; Vasiljeva, O. Differential Impact of Cysteine Cathepsins on Genetic Mouse Models of De novo Carcinogenesis: Cathepsin B as Emerging Therapeutic Target. *Front. Pharmacol.* **2012**, *3*, No. 133.
(40) Lee, S. J.; Jeong, Y. I.; Park, H. K.; Kang, D. H.; Oh, J. S.; Lee, S. G.; Lee, H. C. Enzyme-responsive doxorubicin release from dendrimer nanoparticles for anticancer drug delivery. *Int. J. Nanomed.* **2015**, *10*, 5489−5503.

DOI: 10.1021/acsomega.9b02386
ACS Omega 2019, 4, 18593−18599